J|A|C|S ARTICLES

Published on Web 03/13/2009

Self-Assembly of Janus Cylinders into Hierarchical Superstructures

Andreas Walther,*,† Markus Drechsler,† Sabine Rosenfeldt,‡ Ludger Harnau,§ Matthias Ballauff,‡ Volker Abetz,|| and Axel H. E. Müller*,†

Makromolekulare Chemie II and Physikalische Chemie I, Bayreuther Zentrum für Kolloide and Grenzflächen, Universität Bayreuth, D-95440 Bayreuth, Germany, Max-Planck-Institut für Metallforschung and Institut für Theoretische and Angewandte Physik, Universität Stuttgart, D-70569 Stuttgart, Germany, and Institut für Polymerforschung, GKSS-Forschungszentrum Geesthacht GmbH, D-21502 Geesthacht, Germany

Received November 3, 2008; E-mail: axel.mueller@uni-bayreuth.de; andreas.walther@hut.fi

Abstract: We present in-depth studies of the size tunability and the self-assembly behavior of Janus cylinders possessing a phase segregation into two hemicylinders. The cylinders are prepared by cross-linking the lamella-cylinder morphology of a polystyrene-*block*-polybutadiene-*block*-poly(methyl methacrylate) block terpolymer. The length of the Janus cylinders can be adjusted by both the amplitude and the duration of a sonication treatment from the micro- to the nanometer length. The corona segregation into a biphasic particle is evidenced by selective staining of the PS domains with RuO_4 and subsequent imaging. The self-assembly behavior of these facial amphiphiles on different length scales is investigated combining dynamic light scattering (DLS), small-angle neutron scattering (SANS), and imaging procedures. Cryogenic transmission electron microscopy images of the Janus cylinders in THF, which is a good solvent for both blocks, exhibit unimolecularly dissolved Janus cylinders with a core−corona structure. These results are corroborated by SANS measurements. Supramolecular aggregation takes place in acetone, which is a nonsolvent for polystyrene, leading to the observation of fiber-like aggregates. The length of these fibers depends on the concentration of the solution. A critical aggregation concentration is found, under which unimolecularly dissolved Janus cylinders exist. The fibers are composed of 2−4 Janus cylinders, shielding the inner insoluble polystyrene hemicylinder against the solvent. Herein, the SANS data reveal a core−shell structure of the aggregates. Upon deposition of the Janus cylinders from more concentrated solution, a second type of superstructure is formed on a significantly larger length scale. The Janus cylinders form fibrillar networks, in which the pore size depends on the concentration and deposition time of the sample.

Introduction

In recent years, Janus particles have attracted much attention in nanoscience due to their interesting properties, both for academic as well as for technological reasons.[1−7] In general, Janus structures can be divided into three classes according to their architecture: spherical micelles (3D), two types of cylinders (1D), and sheets or discs (2D)[8] (see Scheme 1). The synthesis of such noncentrosymmetric structures with compartmentalized coronas is a demanding task for the synthetic chemist. Hence, only a few real nanosized polymer-based Janus structures are known in the literature.

Scheme 1. Possible Janus Architectures with Phase-Segregated Shells: (a) Spherical Janus Micelle, (b and c) Two Types of Janus Cylinders, (d and e) Two Types of Janus Sheet/Disc

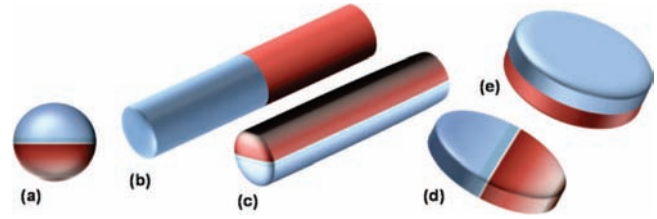

One of the most intensively studied systems is the one concerning the spherical Janus micelles, which are based on template-assisted synthesis using polystyrene-*block*-polybutadiene-*block*-poly(methyl methacrylate) (SBM) block terpolymers. The SBM Janus micelles as well as their amphiphilic pendants, the hydrolyzed SBMA Janus micelles (MA, methacrylic acid), show interesting hierarchical organization on different length scales. The SBM micelles form larger aggregates in nonselective organic solvents, on a silicon surface,[9] and at the air/water interface.[10] The amphiphilic SBMA micelles,

† Makromolekulare Chemie II, Universität Bayreuth.
‡ Physikalische Chemie I, Universität Bayreuth.
§ Universität Stuttgart.
|| Institut für Polymerforschung.

(1) Walther, A.; Matussek, K.; Müller, A. H. E. *ACS Nano* **2008**, *2*, 1167–1178.
(2) Walther, A.; Müller, A. H. E. *Soft Matter* **2008**, *4*, 663–668.
(3) Roh, K.-H.; Martin, D. C.; Lahann, J. *Nat. Mater.* **2005**, *4*, 759–763.
(4) Roh, K.-H.; Yoshida, M.; Lahann, J. *Langmuir* **2007**, *23*, 5683–5688.
(5) Binks, B. P.; Fletcher, P. D. I. *Langmuir* **2001**, *17*, 4708–4710.
(6) Nonomura, Y.; Komura, S.; Tsujii, K. *Langmuir* **2004**, *20*, 11821–11823.
(7) Walther, A.; Hoffmann, M.; Müller, A. H. E. *Angew. Chem., Int. Ed.* **2008**, *47*, 711–714.
(8) Walther, A.; André, X.; Drechsler, M; Abetz, V.; Müller, A. H. E. *J. Am. Chem. Soc.* **2007**, *129*, 6187–6198.

10.1021/ja808614q CCC: $40.75

Scheme 2. Schematic Synthesis of Janus Cylinders

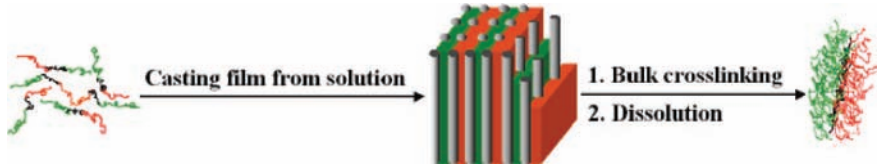

obtained after hydrolysis of the PMMA ester groups, also exhibit superstructures and giant particles.[11] Recently, we succeeded in the preparation of disc-shaped Janus particles which exhibit unexpected back-to-back stacked superstructures in good solvents.[1]

Concerning Janus cylinders, the most promising approach was described by Liu et al., who synthesized Janus cylinders based on the selective crosslinking and subsequent sonication of a lamella-cylinder phase of suitable SBM block terpolymers (see Scheme 1c).[12] Cylindrical Janus structures in the nanometer range are unknown in the literature except for this approach. However, some efforts have been made aiming at the creation of AB-type polymer brushes (see Scheme 1b).[13−15] Besides, different multicompartment particles and internally structured cylinders with higher symmetry, i.e., concentric core−shell−corona-type structures, have been reported by a variety of groups.[16−31]

Janus structures are interesting for a variety of reasons. For instance, they may be used as nanorheological probes, highly specific chemical sensors for immunoassays and molecular interactions, or employed for devices which require switching with an electric or a magnetic field.[32−39] Furthermore, applications are conceivable in fields like nanomedicine. Janus particles with a catalytically active hemisphere exhibit propulsion induced by reactions on one side, resembling to some extent the bacterial flagella.[40,41] In addition, amphiphilic Janus particles could provide an ideal "repair and go" system for cracks within microfluidic channels such as blood vessels and act similar as artificial leukocytes.[42]

Herein, we present results concerning the size tunability of Janus cylinders with compartmentalized corona. Furthermore, structural details of the self-assembly properties of the Janus cylinders will be demonstrated by cryo-TEM, TEM, DLS, and SANS. The studies are fundamentally different from usual self-assembly studies as we analyze the influence of a unique architectural feature, the Janus-type segregation of the cylinder, on the type of aggregates formed. Only by knowing and being able to control the aggregation patterns of subdivided colloids, we will be able to transfer their unique properties into future applications. Aside, Janus cylinders can be considered as a large synthetic analogue of facial amphiphiles, which are of fundamental importance in bioscience. Due to their unique distribution of functional groups on the two sides, they have intriguing properties which result in the formation of distinct colloidal aggregates and foldamers.[43] Thus, studying the aggregate behavior of Janus cylinders can also shine further light on the self-assembly processes in much smaller systems of facial amphiphiles.

Results and Discussion

Size Tunability. Scheme 2 depicts the synthetic procedure toward the preparation of Janus cylinders. The Janus cylinders are produced by the selective crosslinking of the lamella-cylinder morphology, formed by a $S_{41}B_{14}M_{45}^{110}$ block terpolymer (polystyrene-*block*-polybutadiene-*block*-poly(methyl methacrylate)). The indices represent the weight fractions, whereas the superscript shows the overall molecular weight in kg/mol. The

(9) Erhardt, R.; Böker, A.; Zettl, H.; Kaya, H.; Pyckhout-Hintzen, W.; Krausch, G.; Abetz, V. M.; Müller, A. H. E *Macromolecules* **2001**, *34*, 1069–1075.
(10) Xu, H.; Erhardt, R.; Abetz, V.; Müller, A. H. E.; Gödel, W. A. *Langmuir* **2001**, *17*, 6787–6793.
(11) Erhardt, R.; Zhang, M.; Böker, A.; Zettl, H.; Abetz, C.; Frederik, P.; Krausch, G.; Abetz, V.; Müller, A. H. E. *J. Am. Chem. Soc.* **2003**, *125*, 3260–3267.
(12) Liu, Y.; Abetz, V.; Müller, A. H. E. *Macromolecules* **2003**, *36*, 7894–7898.
(13) Ishizu, K.; Satoh, J.; Toyoda, K.; Sogabe, A. *J. Mater. Sci.* **2004**, *39*, 4295–4300.
(14) Lanson, D.; Schappacher, M.; Borsali, R.; Deffieux, A. *Macromolecules* **2007**, *40*, 9503–9509.
(15) Lanson, D.; Schappacher, M.; Borsali, R.; Deffieux, A. *Macromolecules* **2007**, *40*, 5559–5565.
(16) Lodge, T. P.; Bang, J. A.; Li, Z. B.; Hillmyer, M. A.; Talmon, Y *Faraday Discuss.* **2005**, *128*, 1–12.
(17) Lodge, T. P.; Rasdal, A.; Li, Z. B.; Hillmyer, M. A. *J. Am. Chem. Soc.* **2005**, *127*, 17608–17609.
(18) Li, Z. B.; Hillmyer, M. A.; Lodge, T. P. *Macromolecules* **2006**, *39*, 765–771.
(19) Li, Z. B.; Hillmyer, M. A.; Lodge, T. P. *Nano Lett.* **2006**, *6*, 1245–1249.
(20) Li, Z. B.; Kesselman, E.; Talmon, Y.; Hillmyer, M. A.; Lodge, T. P. *Science* **2004**, *306*, 98–101.
(21) Zhong, S.; Cui, H. G.; Chen, Z. Y.; Wooley, K. L.; Pochan, D. J. *Soft Matter* **2008**, *4*, 90–93.
(22) Cui, H. G.; Chen, Z. Y.; Zhong, S.; Wooley, K. L.; Pochan, D. J. *Science* **2007**, *317*, 647–650.
(23) Li, Z. B.; Chen, Z. Y.; Cui, H. G.; Hales, K.; Wooley, K. L.; Pochan, D. J. *Langmuir* **2007**, *23*, 4689–4694.
(24) Li, Z. B.; Chen, Z. Y.; Cui, H. G.; Hales, K.; Qi, K.; Wooley, K. L.; Pochan, D. J. *Langmuir* **2005**, *21*, 7533–7539.
(25) Pochan, D. J.; Chen, Z. Y.; Cui, H. G.; Hales, K.; Qi, K.; Wooley, K. L. *Science* **2004**, *306*, 94–97.
(26) Njikang, G.; Han, D.; Wang, J.; Liu, G. *Macromolecules* **2008**, *41*, 9727–9735.
(27) Stewart, S.; Liu, G. *Angew. Chem., Int. Ed.* **2000**, *39*, 340–344.
(28) Yan, X.; Liu, G.; Haeussler, M.; Tang, B. Z. *Chem. Mater.* **2005**, *17*, 6053–6059.
(29) Yan, X.; Liu, G.; Li, Z. *J. Am. Chem. Soc.* **2004**, *126*, 10059–10066.
(30) Yan, X.; Liu, G.; Liu, F.; Tang, B. Z.; Peng, H.; Pakhomov, A. B.; Wong, C. Y. *Angew. Chem., Int. Ed.* **2001**, *40*, 3593–3596.
(31) Wang, X.; Guerin, G.; Wang, H.; Wang, Y.; Manners, I.; Winnik, M. A. *Science* **2007**, *317*, 644–647.
(32) Behrend, C. J.; Anker, J. N.; McNaughton, B. H.; Kopelman, R. *J. Magn. Magn. Mater.* **2005**, *293*, 663–670.
(33) Choi, J.; Zhao, Y.; Zhang, D.; Chien, S.; Lo, Y.-H. *Nano Lett.* **2003**, *3*, 995–1000.
(34) Anker, J. N.; Behrend, C.; Raoul, K. *J. Appl. Phys.* **2003**, *93*, 6698–6700.
(35) Anker, J. N.; Kopelman, R. *Appl. Phys. Lett.* **2003**, *82*, 1102–1104.
(36) Behrend, C. J.; Anker, J. N.; McNaughton, B. H.; Brasuel, M.; Philbert, M. A.; Kopelman, R. *J. Phys. Chem. B* **2004**, *108*, 10408–10414.
(37) Behrend, C. J.; Anker, J. N.; Kopelman, R. *Appl. Phys. Lett.* **2004**, *84*, 154–156.
(38) Nisisako, T.; Torii, T.; Takahashi, T.; Takizawa, Y. *Adv. Mater.* **2006**, *18*, 1152–1156.
(39) Roh, K.-H.; Yoshida, M.; Lahann, J. *Langmuir* **2007**, *23*, 5683–5688.
(40) Golestanian, R.; Liverpool, T. B.; Ajdari, A. *Phys. Rev. Lett.* **2005**, *94*, 220801.
(41) Howse, J. R.; Jones, R. A. L.; Ryan, A. J.; Gough, T.; Vafabakhsh, R.; Golestanian, R. *Phys. Rev. Lett.* **2007**, *99*, 048102.
(42) Verberg, R.; Dale, A. T.; Kumar, P.; Alexeev, A.; Balazs, A. C *J. R. Soc. Interface* **2007**, *4*, 349–357.
(43) Zhao, Y. *Curr. Opin. Colloid Interface Sci.* **2007**, *12*, 92–97.

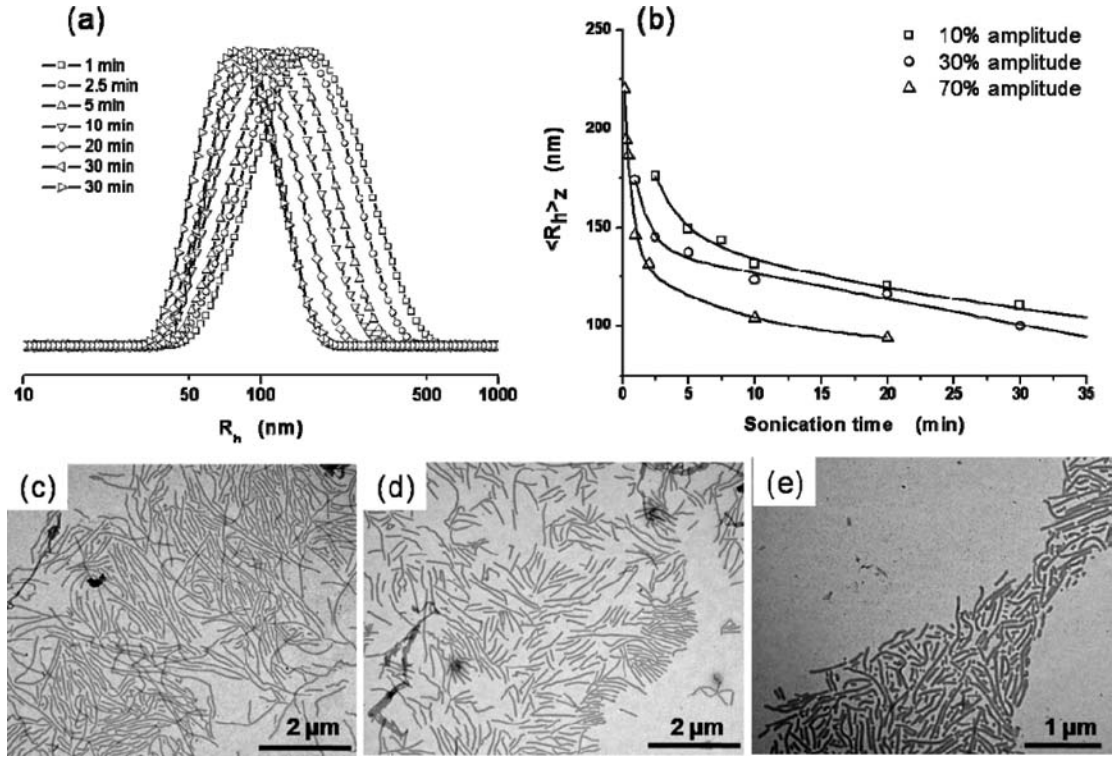

Figure 1. Size evolution of Janus cylinders: (a) DLS CONTIN plots in THF at various states of sonication at 30% sonication amplitude and 80° scattering angle. (b) Time dependence of the apparent z-average hydrodynamic radius, obtained after extrapolating to $q^2 = 0$, at different sonication amplitudes as indicated in the image. (c, d, and e) TEM images obtained for different sonication times at 30% amplitude (1, 5, and 20 min).

crosslinking of the polybutadiene (PB) domains can be accomplished via cold vulcanization using S_2Cl_2 in a well-ordered solvent-swollen bulk morphology.[44]

Since sonication is used to create soluble cylinders from the tightly crosslinked block terpolymer template, it is possible to adjust their length by the duration of the homogenization procedure. Dynamic light scattering (DLS) and transmission electron microscopy (TEM) were used to characterize the size evolution of the Janus cylinders with time and varying power (see Figure 1).

The size distributions obtained by DLS show a characteristic shift toward smaller hydrodynamic radii with increasing sonication time. Besides, the curves exhibit a significant narrowing for longer sonication times, indicating a decrease in polydispersity of the system. The second cumulant, which can be considered as an estimation of the polydispersity of the samples, decreases from 1.3 to 1.1. A detailed look at the evolution of the z-averaged hydrodynamic radius, $\langle R_h \rangle_z$, with sonication time and sonication power reveals a rapid decay. The curves follow an exponential decrease, indicating that in the beginning of the ultrasound treatment the large cylinders are fragmented into significantly smaller ones. After a certain time the curves show a more asymptotical behavior with a slower decay of the cylinder length. Consequently, there is some higher resistance to the introduced sonication energy, due to the higher mobility of smaller structures, and an accompanying higher resistance and more flexible adaptation to the shock waves produced by the ultrasound. An increase in the sonication amplitude from 10% to 70% leads to a faster disruption as more energy is introduced into the system. The observed decrease of the hydrodynamic radius can be correlated convincingly to a shortening of the Janus cylinders as observed by TEM (see Figure 1c−e). The consecutive series of TEM images were obtained from Janus cylinder samples at different sonication times. Whereas the left image shows cylindrical molecules exceeding the 2 μm scale bar, the right image displays cylinders significantly smaller than 2 μm. The image in the center exhibits cylinders of intermediate length corresponding to intermediate sonication time. The results demonstrate convincingly the facile tunability of the size of the Janus cylinders. The cylindrical Janus particles can be adjusted from the micrometer range down to the nanometer level, thus covering a large mesoscopic length scale.

Janus Character. After being able to tune the size by means of sonication, it is of interest to give evidence for the Janus character of the synthesized cylinders. To draw comprehensive conclusions about the self-assembly behavior, knowledge of the cross-section is an important prerequisite. Figure 2 shows several TEM images of Janus cylinders after staining with RuO_4. RuO_4 preferentially stains interfaces and aromatic moieties such as PS, which is one hemicylinder of the Janus cylinders. Note that the PB core remains almost nonstained due to the nearly quantitative consumption of the double bonds during the crosslinking with S_2Cl_2. Prior to staining, a core−corona structure of the cylindrical particles can be found (see Supporting Information, Figure Sup-2). The core has a diameter of ca. 15 nm and is significantly darker due to the presence of S_2Cl_2 within the inner PB cylinder. The overall cylinder diameter reaches a value of ca. 65 nm.

Figure 2 displays the images obtained after staining. Figure 2a shows individual cylinders with a symmetric appearance of the cross-section. This is caused by a thermodynamically preferred adsorption of the nonpolar PS side of the Janus

(44) Walther, A.; Goldel, A.; Müller, A. H. E. *Polymer* **2008**, *49*, 3217–3227.

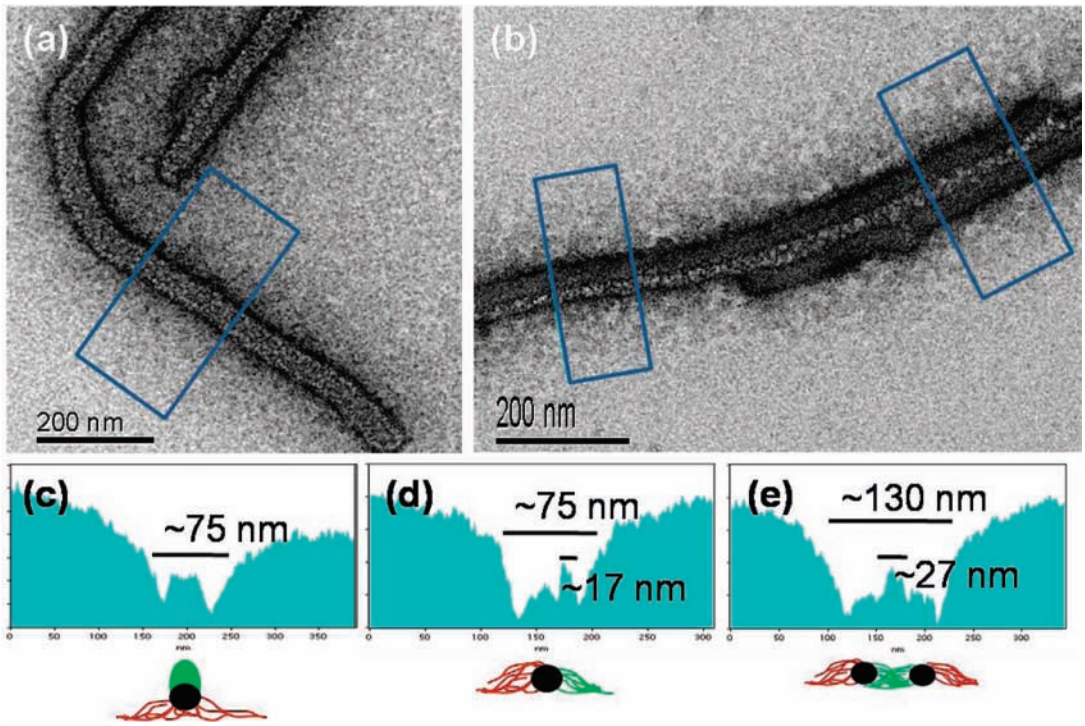

Figure 2. TEM images of single (a) and aggregated (b) Janus cylinders on a carbon-coated TEM grid after staining with RuO_4 for 2 h. Grey-scale analyses (c−e) correspond to the section analyses as shown in the images from left to right. The schematic drawings at the bottom exhibit the orientation of the Janus cylinders within the cross-sections (PB = black, PS = red, PMMA = green).

cylinders onto the carbon film. The diameter of the structure is ca. 75 nm (outer dark lines as margin). The two dark parallel lines indicate the presence of the major amount of polystyrene due to the strong selective staining. PMMA does not lead to any contrast in TEM, as it is nonstained and additionally degrades upon e-beam exposure. Note that a slight dark corona can be seen surrounding the cylinders, which is caused by PS chains adsorbed onto the grid (ca. 20−25 nm). Strong adsorption and introduction of chemical stains (bulky molecules) can alter the dimensions of the particles, and thus, the dimension found may somewhat differ from the ones in solution. The dimensions in solution as obtained by SANS and cryo-TEM will be discussed below.

To be able to visualize the desymmetrized corona, we have to take advantage of the aggregation tendency of Janus cylinders during drying on the surface of the TEM grid. Figure 2b shows a magnified section in which two Janus cylinders are aggregated on the right-hand side of the image. This aggregation of two Janus cylinders induces a rotation of the cylinders on the substrate. Aggregation hinders a preferred adsorption of one of its sides onto the TEM grid. The observation direction is now in plane with the interface of the phase segregation (see schematic drawings at the bottom of Figure 2). The cross-section in Figure 2d corresponds in terms of the diameter to an individual Janus cylinder (∼75 nm) and clearly exhibits a biphasic cross-section. The white part (∼17 nm) corresponds to the PMMA part. This white part is almost doubled (∼27 nm, Figure 2d) between the two aggregated Janus cylinders on the right-hand side of Figure 2b. The two cylinders stick together with their PMMA sides. The overall diameter increases to ca. 130 nm, corresponding to two Janus cylinders. In conclusion, the selective staining of the PS domain of the cylinders clearly confirms the biphasic segregation of the corona into a Janus cylinder. This result also represents one of the first direct real-space proofs for the Janus character of nanosized polymeric colloids, which is often a very challenging task.

Solution Properties and Self-Assembly Behavior. Janus particles are known to undergo unexpected self-aggregation, even in good solvents. Earlier, Erhard et al. demonstrated convincingly that spherical Janus micelles assemble into discrete clusters above a certain critical aggregation concentration.[9] Recently, we published results on Janus discs indicating a back-to-back stacking of the particles in THF.[8] A similar stacking was observed by Lodge for some multicompartment micelles.[18] During the investigation of the disc-like Janus particles it turned out that cryo-TEM in THF is a very powerful technique to investigate the aggregation behavior of labile aggregates in organic solvents.[45] Compared to standard imaging techniques like scanning force microscopy (SFM) or scanning electron microscopy, this in situ technique has major advantages. The first is the fact that the accessible concentration range is typically much higher. In particular, when analyzing the self-aggregation behavior of particles which are supposedly well soluble in the solvent (like a PS-PMMA Janus micelle in THF), the expected critical aggregation concentrations may be rather high. Moreover, the particles may only be loosely bound together. Usually, it is not possible to deposit single and well-separated molecules from more concentrated solution onto grids or wafers for imaging. However, cryo-TEM can directly image relatively high concentrations, and in combination with, e.g., SFM for lower concentrations, a larger concentration range can be covered, leading to the possibility of determining larger aggregation concentrations. The second important advantage is the absence of drying artifacts for cryo-TEM.

(45) Walther, A.; Goldmann, A. S.; Yelamanchili, R. S.; Drechsler, M.; Schmalz, H.; Eisenberg, A.; Müller, A. H. E. *Macromolecules* **2008**, *41*, 3254–3260.

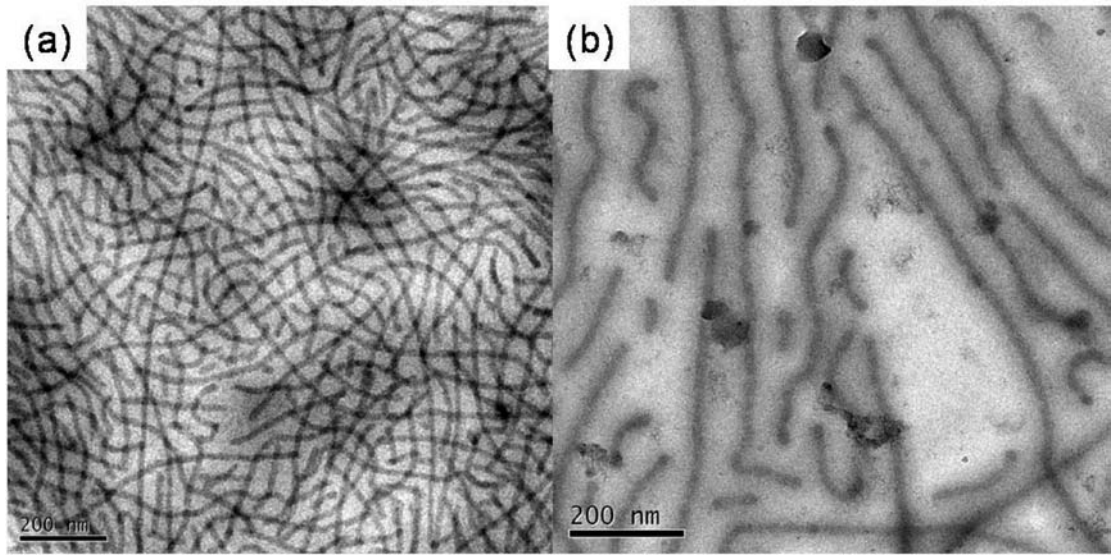

Figure 3. Cryo-TEM images obtained from Janus cylinders in THF at a concentration of 10 g/L. The samples were sonicated for 5 (a) or 2.5 (b) min, respectively.

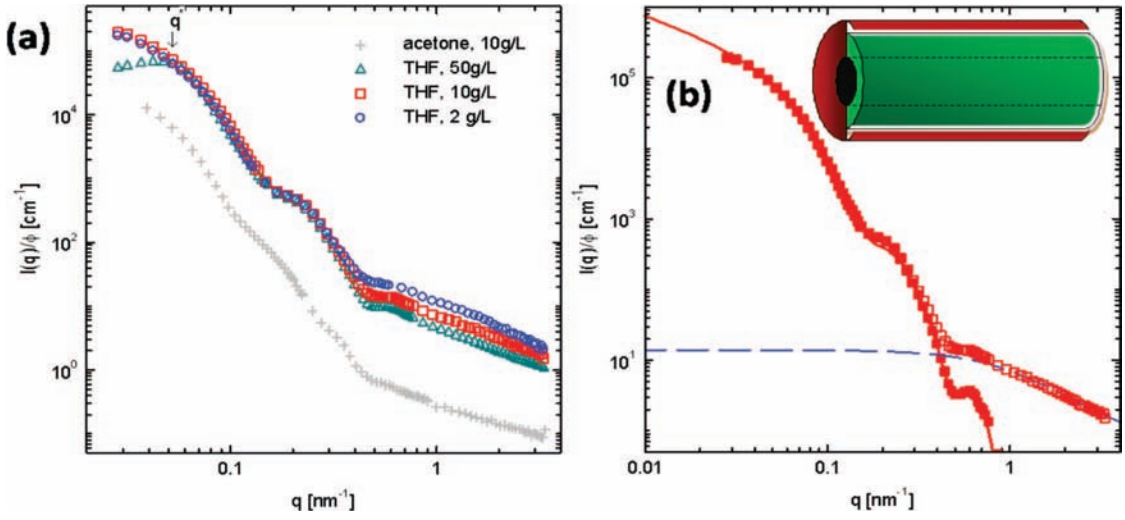

Figure 4. (a) Scattering intensities of the Janus particles in THF normalized to the volume fraction ϕ. The scattering pattern of the Janus cylinders in acetone is shown for comparison and will be discussed below. It is shifted down by a factor of 10. (b) Scattering intensity of Janus cylinders (10 g/L) in THF before (open squares) and after (filled squares) subtraction of the contributions due to concentration fluctuations and incoherent scattering (blue dashed line). The solid line gives the description of the data based on the form factor of Janus cylinders. The inset shows a schematic drawing of the form factor model used.

Due to these advantages, cryo-TEM images of two batches of Janus cylinders with different lengths were acquired (see Figure 3). The images clearly exhibit numerous cylindrical molecules with a random orientation of their major axis. The Janus cylinders are well separated, despite the crowdedness visible in the images. An organization into superstructures is not visible and thus not taking place. This is in contrast to the results obtained for spherical and disc-shaped Janus particles, which showed unexpected aggregates in nonselective organic solvents.

The dark cylinders in all images correspond to the core of the Janus cylinder only. Note that the core has the highest contrast due to the incorporation of a large amount of S_2Cl_2 during the crosslinking procedure. The average core diameter is around 18 nm. The polybutadiene core is slightly swollen by the solvent as TEM investigations of the crosslinked terpolymer bulk structure and the dried cylinder yield a value of 15−16 nm for the crosslinked core diameter. The Janus cylinders exhibit two kinds of endcaps. Hemispherical endcaps, similar to those found for worm-like micelles of diblock copolymers, originate from defects in the bulk morphology. Second, we observe cut endcaps that are created during the ultrasound treatment, in which the particles are chopped into smaller ones. In addition, the Janus cylinders do not show much bending. The stiffness originates from the strong crosslinking of the well-defined initial block terpolymer bulk structure that contained 14 wt % polybutadiene. Note that bending is however restricted into two dimensions as the cylinders are confined within a thin film of vitrified THF. A careful inspection of the cylinders in Figure 3b reveals a core−corona contrast of the Janus cylinders. The cylinders are surrounded by a diffuse corona of side chains. The corona is around 20−25 nm thick and explains the relatively equal spacing between parallel cylinders, which are obviously confined in a very thin vitrified film of THF. Figure 3b gives the indication that the organization into superstructures is prevented by an efficient repulsion of the brush hairs.

The absence of any critical aggregation concentration could furthermore be confirmed by dynamic light scattering (DLS) and small angle neutron scattering (SANS). DLS shows a constant diffusion coefficient (3.25×10^{-15} m^2/ms) in a very large concentration range (10^{-3}−1 g/L) for a chosen sample at 2.5 min sonication at 30% amplitude. The SANS data are shown in Figure 4 and can provide further insights in the solution behavior.

Figure 4a shows the scattering intensities of the system in different solvents. We will first focus on the THF solutions; the scattering pattern in acetone is shown to allow direct and easy comparison later on. All intensities are normalized to the volume fraction, $\phi = \rho V_p$ (ρ is the number density and V_p is the particle volume), of the particles. We attempted to describe the scattering intensity with a model of noninteracting Janus cylinders, as schematically sketched in Figure 4b.

In detail, the scattering intensity of Janus cylinders $I(q,\rho)$ as a function of the scattering vector q ($q = |q| = (4\pi/\lambda)\sin(\theta/2)$, λ is the incident wavelength, and θ is the scattering angle) and the number density, ρ, of the dissolved particles is given by[46−48]

$$I(q,\rho) = \rho I_0(q) S(q,\rho) + I_F(q,\rho) + I_{\text{incoh}} \quad (1)$$

Here $I_0(q)$ describes how the scattering intensity is modulated by interference effects between radiation scattered by different parts of the same particle. Consequently, it is sensitive to the shape of the particle. The structure factor $S(q,\rho)$ is determined by the mutual interactions between different particles. Thus, it depends on the degree of local order in the sample. The contribution to the scattering intensity due to concentration fluctuations of the polymer chains is denoted by $I_F(q,\rho)$. I_{incoh} is the contribution of the incoherent scattering due to the protons. In the present study, the last two contributions become important only for large scattering vectors. I_{incoh} can be assumed to be constant in the given q range.[46,47] The contribution of the concentration fluctuations may be treated within a Gaussian approximation, as follows

$$I_F(q,\rho) = \frac{I_F(0,\rho)}{1 + \xi^2 q^2} \quad (2)$$

where the correlation length ξ decreases upon increasing particle number density according to $\xi \propto \rho^{-1/2}$.[47]

As suggested by the imaging data, the form factor may be best described by a core−shell cylinder with a phase-separated shell as schematically shown in Figure 4b. Therefore, we derived an expression for the scattering intensity of a randomly orientated noninteracting monodisperse Janus cylinder. It is given by (see Supporting Information for further details)

$$I_0(q) = \frac{1}{4\pi}\int_0^{2\pi} d\varphi \int_0^{\theta} d\theta \sin\theta F(q,\theta,\varphi) F^*(q,\theta,\varphi) \quad (3)$$

with

$$\begin{aligned} F(q,\theta,\varphi) &= 2\pi\Delta\rho_c \frac{L_c \sin(q\cos\theta(L_c/2))}{q\cos\theta(L_c/2)} \frac{R_c^2 J_1(qR_c\sin\theta)}{qR_c\sin\theta} + \\ &\quad \frac{L_s \sin(q\cos\theta(L_s/2))}{q\cos\theta(L_s/2)} \\ &\times [\Delta\rho_{sL}\int_0^{\pi} d\varphi_r \frac{1}{A^2}(e^{iAR_{sL}}[1 - iAR_{sL}] - \\ &\quad e^{iAR_c}[1 - iAR_c]) \\ &+ \Delta\rho_{sR}\int_{\pi}^{2\pi} d\varphi_r \frac{1}{A^2}(e^{iAR_{sR}}[1 - iAR_{sR}] - \\ &\quad e^{iAR_c}[1 - iAR_c]) \\ A &= q\sin\theta\cos(\varphi_r - \varphi) \end{aligned}$$

The model accounts for a core−shell cylindrical structure with a core radius (R_c), a certain length of shell and core (L_s, L_c), and a biphasic shell, which has different extensions of the hemishells (R_{sL} and R_{sR}) and unlike scattering length densities ($\Delta\rho_c$, $\Delta\rho_{sL}$, and $\Delta\rho_{sR}$). The grafting nature of the semishells of the particle leads to significantly smaller scattering length densities, $\Delta\rho_{sL}$ and $\Delta\rho_{sR}$, as compared to the bulk phases. This was considered in the fitting of the data. On the basis of the TEM images and well-defined bulk structures used for the preparation of the Janus cylinders, we initially did not expect any significant polydispersity in the radius. However, in solution the soft hemicylinder shells fluctuate significantly, and thus, we had to take a distribution of the radii into account.

The scattering intensities of the Janus cylinders in THF exhibit two oscillations in the intermediate q range. The upturn of the intensity at $q^* \approx 0.05$ nm^{-1} for the concentration of 50 g/L can be attributed to intermolecular correlations between the particles. The mean distance d between two Janus cylinders can be approximated to $d = 130$ nm ($2\pi/q^* = d$). This value is in good agreement with the distance between two particles seen in the cryo-TEM pictures. At intermediate scattering vectors, the scattering intensities measured in THF nearly merge and thus predominantly describe the cross-section of the Janus cylinders. After subtraction of the contributions due to concentration fluctuations and incoherent scattering, the coherent scattering intensity pattern could be recovered (filled symbols in Figure 4b).[46,48]

Due to the polydispersity in the overall radius and the very similar scattering length densities of the two solvent-swollen hemicylinders, we do not detect any difference between R_{sR} and R_{sL}. The best description for single nonaggregated Janus cylinders in a good solvent was obtained for $R_c = 8$ nm, $R_{sL} = R_{sR} = R_s = 27$ nm, corresponding well with the imaging data. A Schulz-Zimm distribution was used to characterize the size distribution of the overall radius ($\sigma_s = 3$ nm in THF). Unfortunately, it is not possible to deduce the length of the Janus cylinders due to the limited q range accessible with SANS.[46,47] The modeling of the SANS data and the deduced length scales corroborate the imaging data and prove that the Janus cylinders are unimolecularly dissolved in good solvents over a wide concentration regime. This is a striking difference as compared to spherical and disc-like Janus particles,[8,9] which showed aggregation patterns in good solvents for both sides.

To introduce a stronger driving force for the self-assembly, the aggregation behavior in acetone was studied. Acetone is a nonsolvent for polystyrene and thus promotes aggregation of the Janus cylinders. Figure 5 shows the concentration-dependent diffusion coefficient of a sample of Janus cylinders, the corresponding CONTIN plots, as well as SANS data and TEM images of the aggregates formed. In contrast to typical DLS

(46) Benoit, H. C.; Higgins, J. S. *Polymers and Neutron Scattering*; Clarendon Press: Oxford, 1994.
(47) Yan, L.; Harnau, L.; Cohen Stuart, M. A.; Rosenfeldt, S. *Soft Matter* **2008**, *4*, 2207–2212.
(48) Rosenfeldt, S.; Dingenouts, N.; Ballauff, M.; Lindner, P.; Likos, C. N.; Werner, N.; Vögtle, F. *Macromol. Chem. Phys.* **2002**, *203*, 1995–2004.

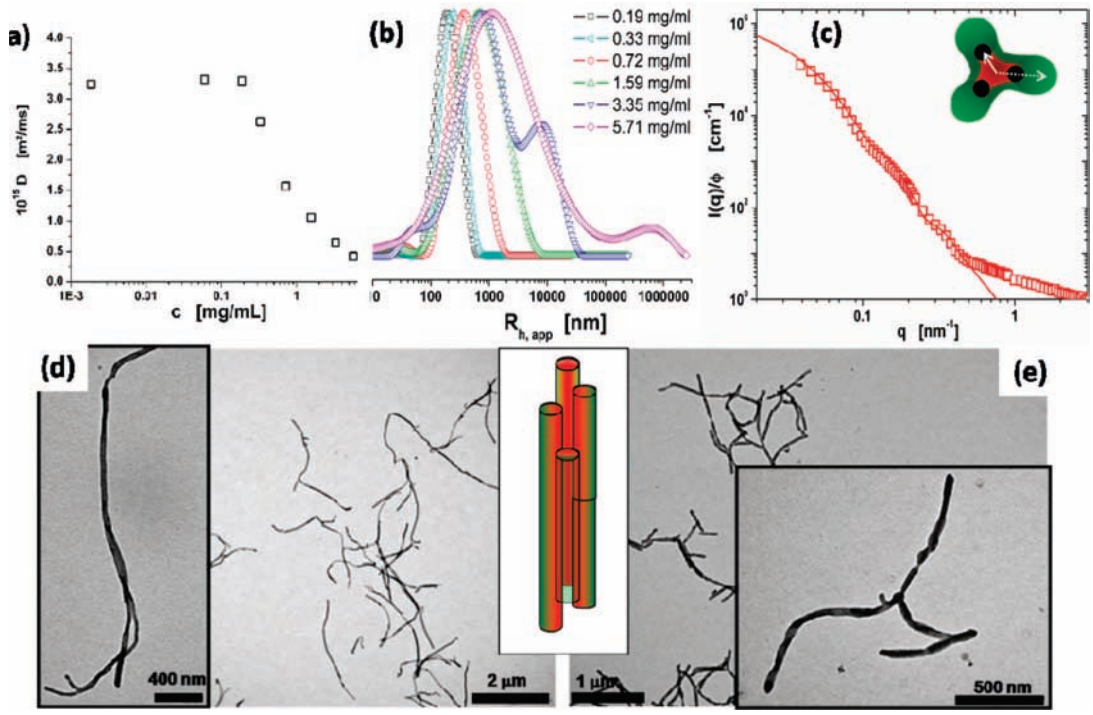

Figure 5. (a) Concentration dependence of the diffusion coefficients of a sample of Janus cylinders (sonication at 30% amplitude for 2.5 min). (b) CONTIN plots at 80° scattering angle at various concentrations, as indicated. CONTIN plots for $c < 0.19$ g/L are omitted, as they coincide with the one of 0.19 g/L. (c) SANS data, modeling, and a schematic cartoon depicting the deduced length scales of a cross-section of one possible aggregate (PS = red, PB core = black, PMMA = green). (d and e) TEM images obtained after deposition from a 0.5 g/L acetone solution of Janus cylinders onto carbon-coated grids after 2.5 (d) and 30 (e) min sonication at 30% amplitude. The two insets show magnified images. The scheme in the center highlights the occurring aggregation. The polystyrene part (red) is hidden within the center of a fiber-like aggregate.

measurements in THF, a clear kink at $c \approx 0.2$ g/L is present for the concentration dependence of the diffusion coefficient. Below this concentration, the diffusion coefficient stays constant. Furthermore, the value coincides with the diffusion coefficient obtained for the same sample in THF at high dilution (3.25×10^{-15} m^2/ms). The drop of the diffusion coefficient above $c \approx 0.2$ g/L indicates that aggregation of the cylinders into significantly longer structures must take place above this critical aggregation concentration (cac). The clustering of the cylinders into larger aggregates is also evident from the CONTIN plots shown in Figure 5b. The main peak shows a strong shift toward higher radii and even becomes bimodal for higher concentrations, showing the presence of very large structures. The more concentrated solutions show a visible but not a too strong sedimentation after several weeks, meaning that the large structures are reasonably stable.

The SANS intensities, measured in acetone, show a distinct shift of the characteristic oscillations to smaller scattering vectors (Figure 4a) and accordingly an increase of the cross-sectional diameter of the investigated structure. Considering that the PS side is insoluble and no longer solvent swollen in acetone leads to the conclusion that the scattering length densities of the PB core and the PS part become virtually indistinguishable in the experiment. The PS parts shrink into a much more compact substructure and fuse in terms of scattering contrast with the PB core. Thus, R_c should be significantly higher as compared to the Janus particles dissolved in THF. Modeling of the scattering intensity leads to $R_c = 14$ nm and $R_s = 34$ nm (see solid and dotted white line in the scheme in Figure 5c). The fitting includes a polydispersity of $\sigma_s = 7$ nm, being larger than for the individually dispersed cylinder in THF. Hence, the data must be interpreted as an aggregation of several Janus cylinders into a superstructured fiber as sketched within Figure 5c. The moderate expansion of the core diameter R_c is caused by the collapse of the PS part onto it. The radius of the shell increases due to the clustering of several Janus cylinders.

Unfortunately, we failed to obtain cryo-TEM images from acetone solutions. This is probably due to the fast evaporation and poor film-forming properties of acetone. Therefore, standard TEM analysis of the acetone solution of the Janus cylinders was performed. Figure 5 shows a selection of TEM images obtained from self-assembled Janus cylinders at different sonication times, deposited from a 0.5 g/L solution. The images exhibit superstructures formed by the solvent-induced self-assembly. The aggregates remain intact during deposition on the TEM grid, indicating a strong association of the cylindrical Janus particles. The Janus cylinders form fiber-like aggregates with the PS part hidden in the center of the aggregate. The fibers are longer than the initial cylinders in THF but are of finite size. The images reveal that 2−4 Janus cylinders participate in the formation of one superstructured fiber at a given point. The diameters determined by TEM (50−80 nm) are in agreement with the shell thickness derived by modeling the SANS data. The aggregation pattern is independent of the Janus cylinder length as similar aggregates can be found as shown in Figure 5. An increase in the height profile of Janus cylinders deposited from acetone solutions in scanning force microscopy investigations was reported by Liu et al.[12] However, here we look in much more detail at the aggregation patterns, concentrations, and structures formed. TEM images at higher concentration show slightly thicker and much longer fibers, which can explain the further decrease of the diffusion coefficient for solutions with increasing concentration. At very low concentrations, below the cac, unimolecularly and only slightly aggregated Janus

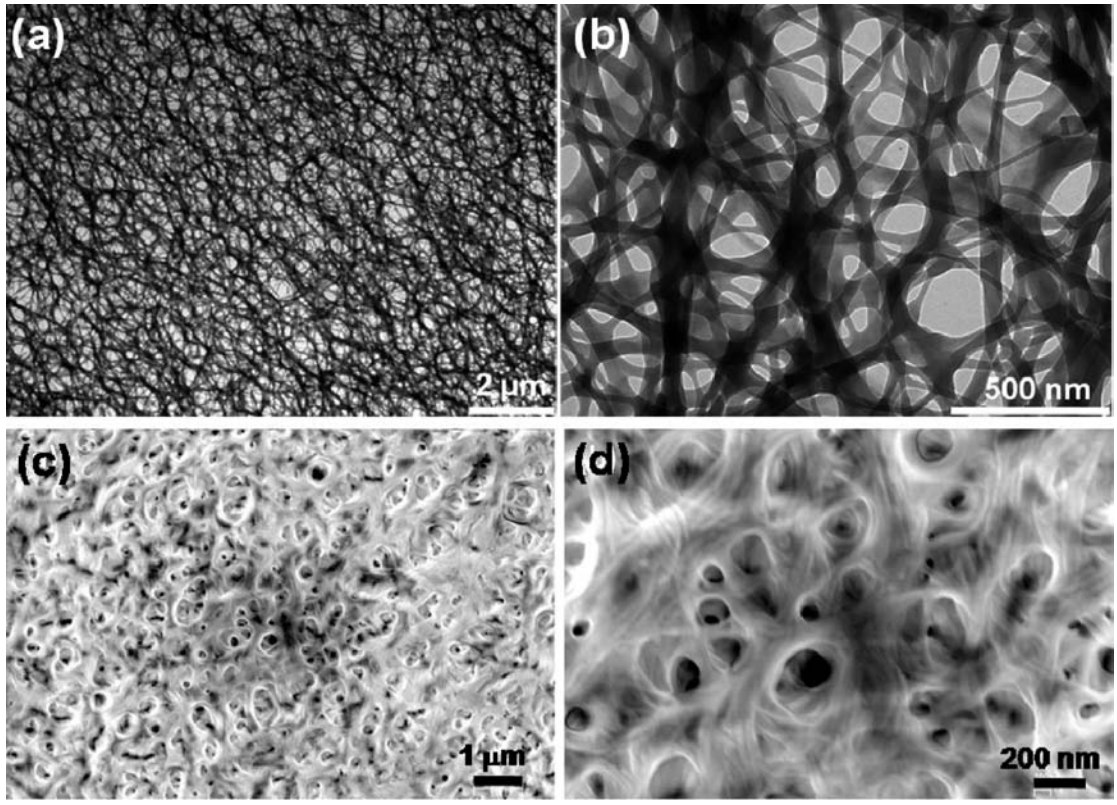

Figure 6. TEM images (a and b) of network-like aggregation patterns formed by deposition of Janus cylinders onto a TEM grid from THF solution (c = 5 g/L). SEM images obtained by drying a solution of Janus cylinders in THF on a mica substrate. (d) Magnified section of image c.

cylinders can be found (see Supporting Information for TEM images). A longitudinal extension of the Janus cylinders is not found. Consequently, since the PS is collapsed in acetone, the PMMA part shields the complete structure and prevents aggregation at such low concentrations. Above the cac, the cylinders are clearly fused together into one homogeneous structure.

The overall picture emerging from the experimental results of the solvent-induced self-assembly of the Janus cylinders in selective solvent is as follows: The aggregation is concentration dependent and shows a critical aggregation concentration. Therefore, the stabilization occurs with two different mechanisms. At very low concentrations, below the cac, the Janus cylinders exist unimolecularly dissolved with a collapsed PS part, which is shielded by the well-soluble PMMA arms in an intramolecular fashion. Around the cac, aggregation takes place by clustering of Janus cylinders, first into aggregates with increased diameter and without significant longitudinal extension. At this point a strong drop in the diffusion coefficient is not expected as an increased diameter has only a minor influence on the overall diffusion coefficient. For energetic reasons, it is favored to start the aggregation with a maximum of contact surface between the PS parts of different cylinders. Above the cac, or more precisely above the kink in Figure 5a, a concentration-triggered fiber-like aggregation into longitudinally extended superstructured fibers takes place. The fibers become longer with increasing concentration. Above the cac, the stabilization involves an intermolecular process in which several cylinders come together and cooperatively shield the inner PS domain.

Surface Structures. Aside from these fiber-like aggregates found in selective solvents, a formation of networks was observed upon depositing Janus cylinders from more concentrated solution. The length scales involved here significantly exceed those of the superstructures formed in dilute and semiconcentrated acetone solution. Consequently, the Janus cylinders can be considered to be able to assemble on a second hierarchical level into considerably larger structures than those formed in selective solvents in dilute and semidilute solution. The aggregation patterns develop in nonselective (THF) and selective solvents (acetone). They can be created in a very facile fashion. Figure 6a and 6b shows representative images obtained by TEM. The network shows polydisperse pores in the range of a few hundred nanometers, which can be developed over a large micrometer-sized area. Thus, the nanoscopic pores can be created over mesoscopic length scales. The pore sizes of these patterns can be tuned in a very simple fashion by increasing the concentration of the solution or the aspiration time. The SEM images shown in Figure 6c and 6d were obtained by drying a droplet of a Janus cylinder solution in THF on a mica substrate. The pores are significantly smaller, in the range of 100−200 nm, and the polymer matrix is more continuous, suggesting a higher mechanical strength. Strikingly, a continuous film formation is not observed, and stabilization of the network-like pattern is favored. The structures found are reminiscent of Bates' work describing the irregular network formation of branched, cylindrical micelles in a certain composition range.[49,50] Whereas the cylindrical micelles may fuse together with their cores therein, here the particles are held together in the network-like structure via their corona blocks, allowing an easy disintegration.

(49) Jain, S.; Dyrdahl, M. H. E.; Gong, X.; Scriven, L. E.; Bates, F. S. *Macromolecules* **2008**, *41*, 3305–3316.
(50) Jain, S.; Gong, X.; Scriven, L. E.; Bates, F. S. *Phys. Rev. Lett.* **2006**, *96*, 138304.

Due to the fiber formation in acetone, with PS being in the center of the superstructured fibers, it is furthermore possible to tune the surface energy of the networks. Whereas a mixed surface of PS and PMMA should be present when creating these patterns with a THF solution, the surface presumably consists exclusively of PMMA when using an acetone solution. This shows a way to tune the surface energy and the chemoselectivity of the structure, which would, for instance, play a role when using these membrane-like structures as templates for atomic layer deposition (ALD) or for further chemical modifications.[51] Furthermore, these structures are appealing when thinking about creating them in polymer matrixes. The networks could be valuable for reinforcing mechanical properties of certain polymers or could be used to create bicontinuous patterns. Selective etching as, for instance, for PMMA with UV irradiation may even be a tool to create nanoscopic channels within a polymer host material (e.g., PS).

Conclusions

We presented a thorough investigation of the size tunability and self-assembly properties of Janus cylinders. The size of the Janus cylinders can be tuned from the micrometer range down to the nanometer range by a simple sonication treatment. The evolution of the particle size follows an exponential decay. The Janus cylinders are unimolecularly dissolved in good organic solvents as observed by cryo-TEM, DLS, and SANS in THF. Cryo-TEM shows a core−corona structure with an extended corona, indicating an efficient repulsion of the brush hairs, which prevents the aggregation into superstructures. The form factor for a core−shell Janus cylinder was developed and used for the fitting process of the SANS data, yielding the dimensions of the particle cross-section. Self-assembly of Janus cylinders can be induced in selective solvents. DLS demonstrates that the aggregation is concentration dependent, exhibiting a critical aggregation concentration (cac), and that the size of the aggregates increases with increasing concentration. Above the cac, the Janus cylinders cluster and form superstructured fibers with a PS domain in its center. The modeling of the SANS data reveals a collapse of the PS part onto the PB core and an aggregation into larger diameters. These data are corroborated by TEM images showing that 2−4 Janus cylinders form one fiber at a given point. Below the cac, the stabilization occurs via an intramolecular mechanism. The collapsed PS side is shielded by the PMMA arms extending around large parts of the cylinder and minimizing the contact between PS and solvent. Aggregation on a second hierarchical level can be obtained when depositing Janus cylinders on surfaces. It is possible to form a network-like pattern upon deposition from concentrated solution, independent of the solvent used. These fibrillar networks can be obtained with different pore sizes and different surface compositions simply by changing the concentration and the solvent quality, respectively.

Acknowledgment. This work was supported by the European Science Foundation within the EUROCORES SONS program (BioSONS) and the EU within the Marie Curie RTN POLYAMPHI. A.W. thanks the Bavarian Graduate Support Program for a scholarship. We are also indebted to the Institut Laue-Langevin (ILL) Grenoble and Peter Lindner for providing beam time and support at the SANS instrument D11.

Supporting Information Available: Experimental part, treatment of the SANS data, and additional experimental data. This material is available free of charge via the Internet at http://pubs.acs.org.

JA808614Q

(51) Puurunen, R. L. *J. Appl. Phys.* **2005**, *97*, 121301.